A Passive Smart Face Mask for Wireless Cough Monitoring: A Harmonic Detection Scheme With Clutter Rejection

Liang Zhu, *Student Member*, *IEEE*, Trung Dũng Hà, *Student Member*, *IEEE*, Yi-Huan Chen, Haiyu Huang, and Pai-Yen Chen, *Senior Member*, *IEEE*

***Abstract*—Cough detection has aroused great interest because the assessment of cough frequency may improve diagnosis accuracy for dealing with several diseases, such as chronic obstructive pulmonary disease (COPD) and the recent COVID-19 global pandemic crisis. Here, we propose and experimentally demonstrate a wireless smart face mask based on a passive harmonic tag for real-time cough monitoring and alert. Our results show that the cough events can be successfully monitored through non-contact track of the received signal strength indicator (RSSI) at the harmonic frequency. Owing to the frequency orthogonality between the launched and backscattered radio-frequency (RF) signals, the harmonic tag-based smart mask can well suppress the electromagnetic interferences, such as clutters and crosstalks in noisy environments. We envision that this zero-power and lightweight wireless wearable device may be beneficial for cough monitoring and the public health condition in terms of tracking potential contagious person and virus-transmissive events.**

***Index Terms*—Antennas, cough monitoring, electromagnetic interferences, harmonic RFID, wearable devices, wireless sensors, smart face mask.**

I. Introduction

COUGH, an expiratory maneuver against a closed glottis with characteristic sound, is a common and important symptom in many respiratory diseases, such as pneumonia and tuberculosis [1], [2]. Cough may appear sporadically with illnesses (e.g. colds and flu) to act as a protective and clearing mechanism, but when it becomes chronic, it could severely impair life quality by interfering with breathing, sleep and normal daily activities [3]-[5]. As a result, this symptom is the commonest reason for people seeking medical advice, and the assessment of cough frequency is considered as a critical tool in clinical use. More urgently, as the disastrous spreading of COVID-19 in 2020, the whole world is in demand of some type of affordable, rapid and effective facilities for warning of transmissive events, identifying potential contagious persons, as well as tracking face-mask wearing compliance in public [6]. Cough, which is one of the top symptoms associated with COVID-19, could be of high interest in being monitored, so as to facilitate the above-mentioned demand in the critical pandemic situation.

Driven by this demand, some attempts to monitor cough have been made, which started around the 1950s with simple audio recording systems that require manual interpretation of cough events [7]. To date, many emerging cough monitoring systems have been developed [8]-[10], which can be divided into three main categories. The first one reached from the airflow measurement requires placing detection module (e.g., piezoelectric sensor) close to the nose or mouth to obtain the flow dynamics of cough [11], [12]. This method is clearly not suitable for continuous cough monitoring in the outpatient environment [13]. The second type is based on monitoring the movement of the chest or abdominal wall [14]. In this approach, an accelerometer is directly placed at the volunteer's chest wall to record cough events. Although this solution can offer precise measurement results, it typically requires a trained operator to manually identify cough events, which is a rather time-consuming and arduous task [14]. The third one based on the measurement of cough sounds has been more universal because of advances in computer technology and the availability of portable digital sound recording devices [15], [16]. Unfortunately, these automatic cough monitors may suffer from confusion with surrounding noises and other parasitic patient sounds (e.g., throat clearing, humming, or laughing) that are not associated with the disease transmissive event. In addition, cough detection using sound could lose important detailed information, e.g. whether the person is wearing a face mask when coughing.

Very recently, several radio-frequency (RF) approaches, such as antenna sensors and passive radio frequency identification (RFID) [17], [18], have been explored for remotely detecting and monitoring cough events [19], [20]. Despite the improved effectiveness, these backscattering tags are often vulnerable to a low signal-to-clutter/noise ratio in noisy indoor environments, thereby impeding real-time, continuous and accurate monitoring of coughs. Seeking to overcome the troublesome issues of passive RF sensing [21],

L. Zhu, T. D. Ha, Y. H. Chen and P. Y. Chen are with the Department of Electrical and Computer Engineering, University of Illinois, Chicago, IL 60607, USA.

H. Huang is with Maxim Integrated Inc., Dallas, TX 75254 USA.

Corresponding authors: P. Y. Chen; e-mail: pychen@uic.edu

This material is based upon work supported by the National Science Foundation under Grant No. 1914420 (ECCS-CCSS program).

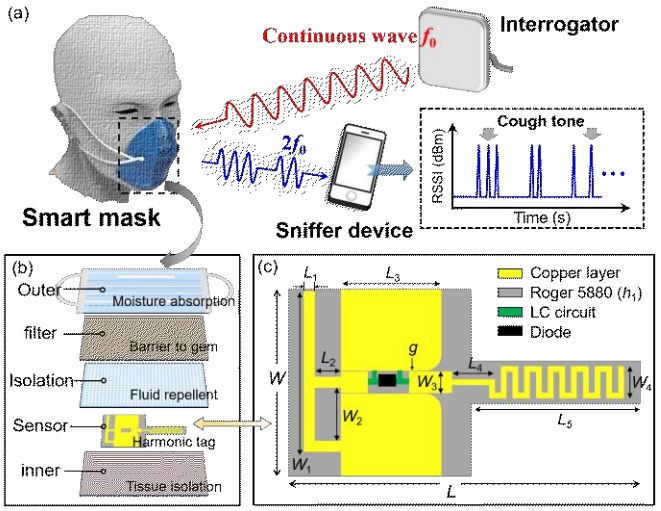

Fig. 1. (a) Schematics of the smart face mask based on a passive, lightweight, and low-profile harmonic tag. (b) Exploded view of the wireless smart face mask. (c) Geometry of the harmonic tag embedded in the face mask.

the harmonic transponder sensor (or harmonic sensor) has been recently proposed [22]-[27]. Similar to the harmonic radar invented in 70s [28], a harmonic sensor launches and detects RF signals at orthogonal frequencies (e.g., fundamental frequency and harmonics) [29]-[33], with the information of sensor encoded in the frequency-modulated RF signal, for avoiding multipath interferences, clutters, and crosstalks [34]-[36]. To date, harmonic sensors have been used to remote sensing of mechanical cracks [37]-[41], humidity [42], liquid levels [43], pH [44], vital signs [45] and biochemical processes [46], as well as localization of underground buried assets [47].

In this work, we propose a lightweight harmonic sensor that can be flawlessly embedded in the face mask to perform rapid, real-time wireless cough monitoring. The harmonic sensor system is sketched in Fig. 1(a). The reader transmits a continuous-wave (CW) RF signal at frequency f_0 to the smart face mask. When the face mask is in close contact with or the proximity of mouth (i.e., air gap $g \sim 0$), the dielectric loading effect due to human tissues will shift resonant frequencies of antennas and, therefore, no detectable harmonic signal can be generated. In other words, the smart face mask is in the OFF state with zero second-harmonic RSSI. On the other hand, when cough happens, the effect of human body disappears (i.e., $g >$ 10 mm) and, thus, the RF monotone can be received by the antenna on the face mask, undergoing the frequency multiplication process ($f_0 \rightarrow 2f_0$), and being re-transmitted to the reader or sniffer. As a result, the harmonic tag can be waked up (i.e., ON state) due to coughs, whose frequency and pattern can be retrieved from the time series of the RSSI at the second-harmonic frequency [Fig. 1(a)]. More interestingly, if the proposed smart face mask becomes a universal standard, combining with sound-based cough monitoring, it can serve as a face mask compliance tracker. For example, if the sound monitoring detects a cough event without a matched RF harmonic, it means that the person who coughs is not wearing a face mask, and it will be alerted as a high-risk event.

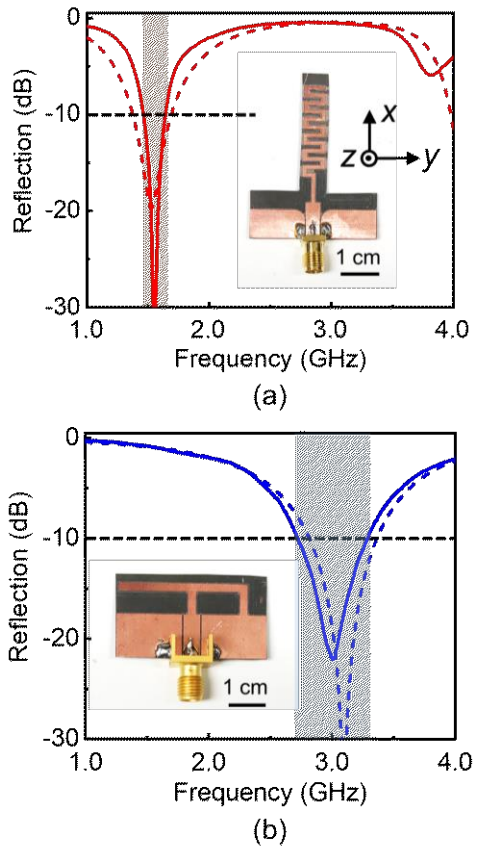

Fig. 2. Measured (solid line) and simulated (dashed line) reflection coefficient versus frequency for (a) the meander-line antenna and (b) the printed inverted-F antenna.

TABLE I
Summary of dimensions in the harmonic tag (units: millimeters)

Par.	L	L_1	L_2	L_3	L_4	L_5
Value	65	2	5	18.8	8	31.5
Par.	W	W_1	W_2	W_3	W_4	g
Value	35	30	10	4	6	0.2

II. Design and Measurement of a Harmonic Tag

Fig. 1(b) depicts the exploded view of the proposed smart face mask, which consists of a harmonic transponder sandwiched between a typical face mask and a tissue isolation layer. Due to the limited area of the face mask, the primary design focus is to find an RF circuit that can fit into a small area on the interior of the face mask, while maintaining excellent sensitivity to human-based dielectric loading. Fig. 1(c) illustrates the top view of the proposed harmonic transponder comprising a meander-line antenna operating at 1.5 GHz (0.26 $\lambda_0 \times 0.175\ \lambda_0 \times 0.0025\ \lambda_0$), a lumped element-based frequency multiplier, and an inverted-F antenna at 3.0 GHz (0.2 $\lambda_0 \times 0.35\ \lambda_0 \times 0.005\ \lambda_0$); the important design parameters are summarized in Fig. 1 and Table I. These components are connected through the coplanar waveguide (CPW) transmission line with a characteristic impedance of 50 Ω. This harmonic transponder was fabricated on the flexible, single-side Roger 5880 substrate with relative permittivity $\varepsilon_r = 2.2$, loss tangent $\delta = 0.0009$, and

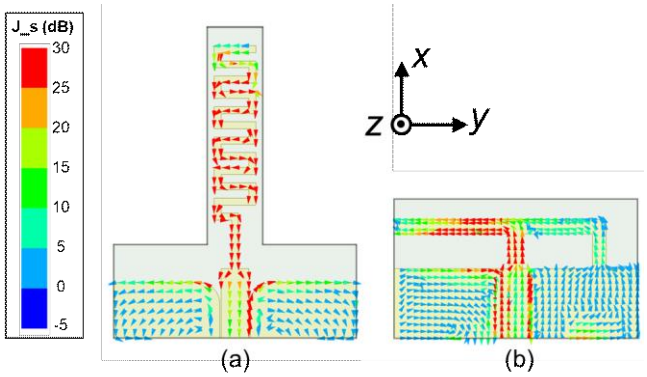

Fig. 3. Surface current distribution of (a) the meander-line antenna at 1.5 GHz and (b) the inverted-F antennas at 3.0 GHz.

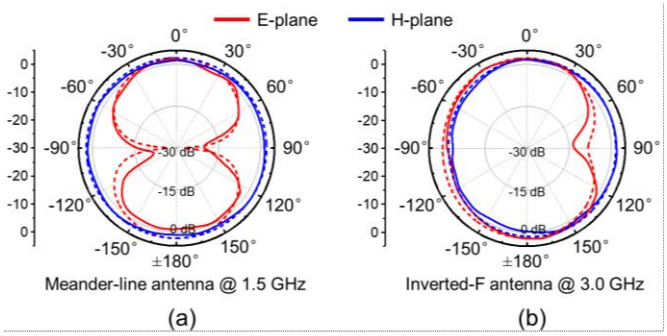

Fig. 4. Measured (solid line) and simulated (dashed) radiation patterns for (a) the meander-line antenna at 1.5 GHz and (b) the printed inverted-F antenna at 3.0 GHz on the E-plane (*x*-*z* plane) and H-plane (*y*-*z* plane).

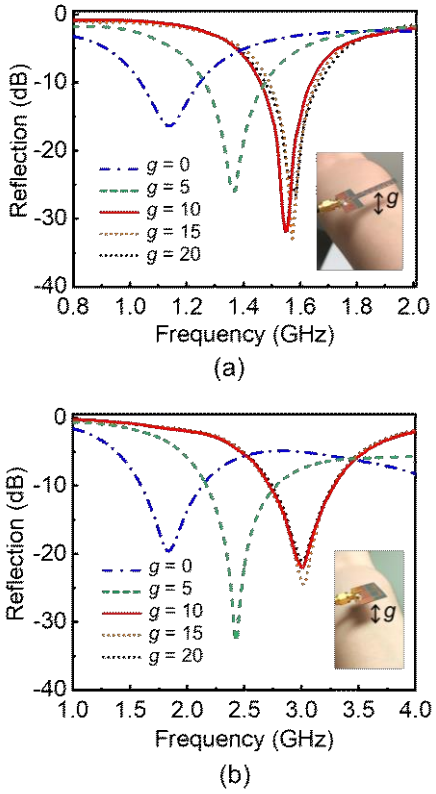

Fig. 5. Measured reflection spectra for (a) the meander-line antenna and (b) the inverted-F antenna, as a function of the dimension of gap (*g* [mm]) between the antenna and human body; the insets show the photograph of the measurement setup.

thickness of only 0.5 mm. The total dimension of the harmonic tag can fit into a small area on the interior of the face mask. Figs. 2(a) and 2(b) report the measured reflection coefficient (S_{11}) and photographs for the microstrip meander-line and inverted-F antennas, respectively. We find that in free space, the meander-line antenna resonates at 1.5 GHz (fundamental frequency) with a -10 dB bandwidth of 164 MHz, while the inverted-F antenna operates at the second-harmonic frequency (3.0 GHz) with a -10 dB bandwidth of 555 MHz. The measurement results are in good agreement with the simulation results, with a fractional frequency shift of 1.33% for the meander-line antenna and 2.28 % for the inverted-F antenna, due primarily to the fabrication errors and variations in the dielectric constant of the substrate. Figs. 3(a) and (b) present the simulation results for the current flow for the meander-line antenna and IFA at 1.5 GHz and 3.0 GHz, respectively, in which it can be seen obviously that at 1.5 GHz, the maximum currents present along the meander-line, and at the second harmonic frequency (3.0 GHz), the resonating current path is observed on the IFA.

Fig. 4 reports the simulated and measured radiation patterns of the meander-line and inverted-F antennas in Fig. 2 at their resonant frequencies. It is evident that the measured radiation patterns are in good agreement with the simulated ones on the E-plane (*x*-*z*-plane) and H-plane (*y*-*z* plane). The meander line antenna exhibits an omnidirectional radiation property at 1.5 GHz, with the maximum measured gain of 2.1 dBi and the half-power beam width (HPBW) of 95° on the E-plane. The inverted-F antenna has the maximum gain of 2.45 dBi at 3.0 GHz, with the HPBW of 105° on the E-plane. Both antennas have the radiation efficiency greater than 85 % at the resonant frequency. Specifically, the meander-line antenna has a radiation efficiency 92 % at 1.5 GHz, and the inverted-F antenna has a radiation efficiency 94 % at 3.0 GHz

Next, we will report the effect of human body on radiation properties of the wearable antennas in Fig. 2. In our experiment, the antenna was placed in the vicinity of human body (hand tissues), and the air gap (*g*) between the antenna and the tissues was varied from 0 mm (i.e., attached onto the skin) to 20 mm. The antenna was connected to the Agilent N5222A PNA microwave network analyzer to track variations of the resonant frequency with the air gap size. Fig. 5(a) reports the measured reflection spectra of the meander-line antenna in Fig. 2(a), showing that when the antenna moves toward the human body, the resonant frequency decreases from 1.5 GHz to 1.15 GHz. Moreover, there is a threshold, g = 10 mm, beyond which the resonant frequency is nearly unchanged and locked at 1.5 GHz. In the same vein, as can be seen in Fig. 5(b), the resonant frequency of the inverted-F antenna in Fig. 2(b) is downshifted from 3.0 GHz to 1.6 GHz in response to reduction of air gap, with a threshold distance, g = 10 mm. According to the cavity perturbation theory, the downshift of resonant frequency in response to dielectric perturbations is proportional to the perturbed field strength [48], [49]. Therefore, due to strong electric fields in the close vicinity of the antennas, any change

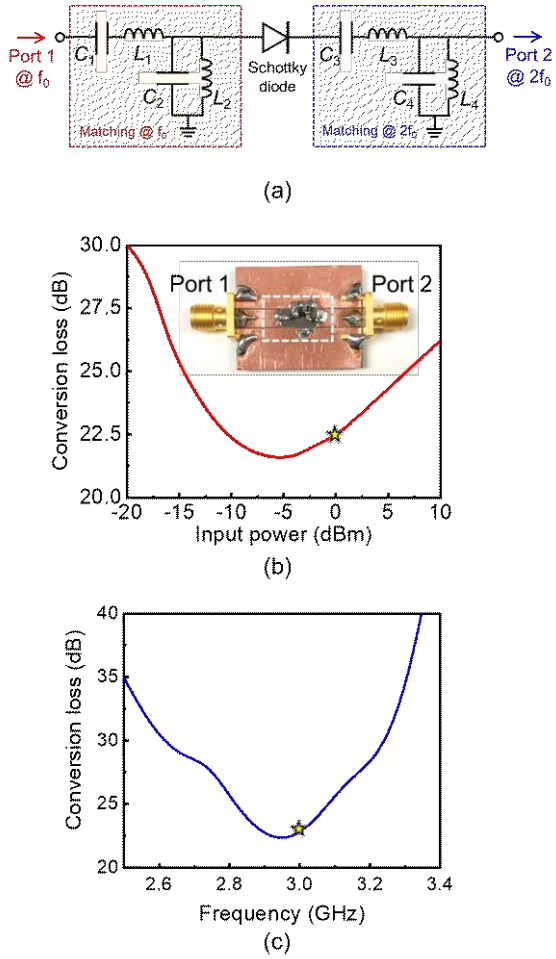

Fig. 6. (a) Circuit diagram of a lumped element-based frequency doubler, and its measured conversion loss in dB (b) at different input power levels (f_0 = 1.5 GHz) and (c) at different input frequencies (1.25 GHz ≤ f_0 ≤1.7 GHz).

TABLE II
Parameters of lumped elements with units: C (pF) and L (nH)

Par.	C_1	L_1	C_2	L_2	C_3	L_3	C_4	L_4
Value	10	22	3.3	3.9	1.8	1.5	10	33

in the air gap, if within 10 mm, could cause a remarkable resonant frequency shift. On the contrary, if the antenna is away from tissues, the resonant frequency is nearly independent of the air gap size. When the antennas are utilized in the harmonic tag inside the face mask, their resonant frequencies may be significantly detuned under the normal wearing condition (g < 5 mm). However, when cough happens, the space between the antenna and facial surface increases (g > 10 mm) and, therefore, the operating frequencies of the meander-line and inverted-F antennas may be reconfigured to the fundamental and second-harmonic frequencies (i.e., 1.5 GHz and 3.0 GHz). In this scenario, a second-harmonic RSSI can be detected by the reader or sniffer in the far zone.

Fig. 6(a) shows the schematic diagram of a miniaturized frequency doubler, whose input and output ports are connected to the meander-line antenna and the inverted-F antenna. In order to save the area of harmonic tag, the bandpass filters and matching networks were constructed by lumped elements and a Schottky diode (SMS 7621), with the important design

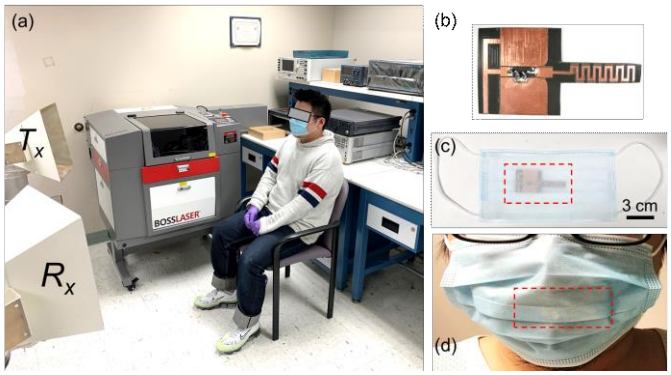

Fig. 7. (a) Wireless cough monitoring (bistatic configuration) in an indoor environment. Photographs of (b) the passive harmonic tag, (c) the assembled smart face mask, and (d) the smart face mask worn by the user.

parameters listed in Table II. The passbands of the *LC* band-pass filters on the input and output sides are centered at 1.5 GHz and 3.0 GHz, respectively. The Advanced Design System (ADS) was utilized to design the frequency doubler [50]. The photograph of the fabricated frequency doubler is shown in the inset of Fig. 6(b). Fig. 6(b) reports the measurement results for the relationship between the conversion loss and input RF power at 1.5 GHz. We find that at the 0 dBm input level, the conversion loss is ~22.5 dB. Fig. 6(c) reports the measurement results for the conversion loss versus the second-harmonic frequency at input power of 0 dBm. The frequency dependency shows that the minimum conversion loss (~22.5 dB) was obtained at 3.0 GHz. The conversion loss of the lumped element-based frequency doubler is also sensitive to human tissues. When g ~ 0, the conversion loss is reduced to 40 dB, due primarily to the impedance mismatch between the CPW transmission line and the input/output port of the frequency doubler, as well as the increased dielectric loss.

Finally, the afore-studied antennas and frequency multiplier were integrated to make a passive harmonic transponder [Fig. 1(c)]. This compact, low-profile passive harmonic tag was sandwiched between a typical face mask and a protection layer to form a smart face mask for wireless cough monitoring applications [Fig. 1(b)]. For this proof-of-concept demonstration, we mainly focus on implementing and testing the effectiveness of the smart face mask based on the passive harmonic transponder. The fundamental frequency and second harmonic frequency are 1.5 GHz and 3.0 GHz, respectively. However, this concept can be readily extended to any type of antenna that is small enough for mask assembly and sensitive to the human body-based dielectric loading effect. Hence, the concept can be applied to any frequency band of interest by properly scaling the antenna and circuits.

III. Wireless Smart Face Mask for Cough Monitoring

We adopted the bistatic measurement setup in a cluttered indoor environment, as illustrated in Fig. 7(a). Figs. 7(b)-(d) present the photographs of the fabricated passive harmonic transponder, the assembled smart face mask, and a user wearing the smart face mask, respectively. During the measurement, the reader's transceiver continuously launches an CW interrogation signal (at 1.5 GHz) to the user wearing the smart face mask. The

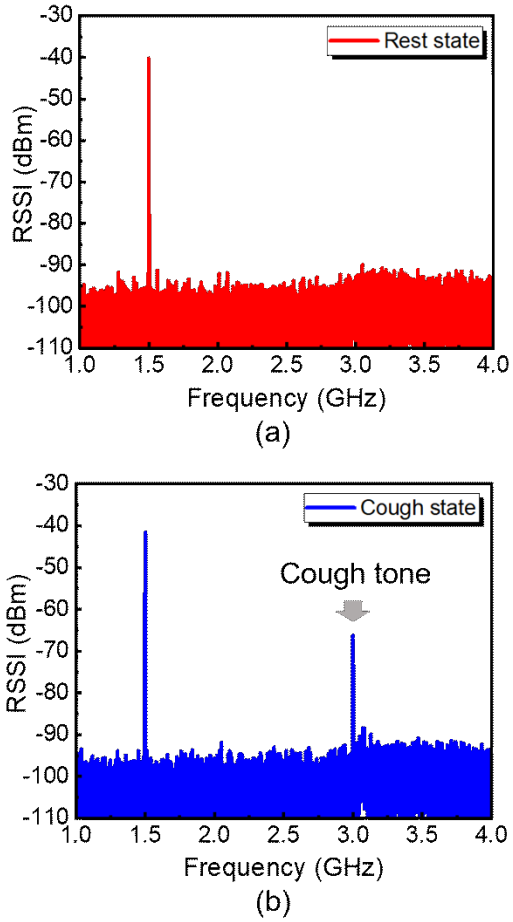

Fig. 8. Measured RSSI in the physical state of (a) peaceful rest and (b) cough; the interrogating signal is an unmodulated CW carrier at 1.5 GHz.

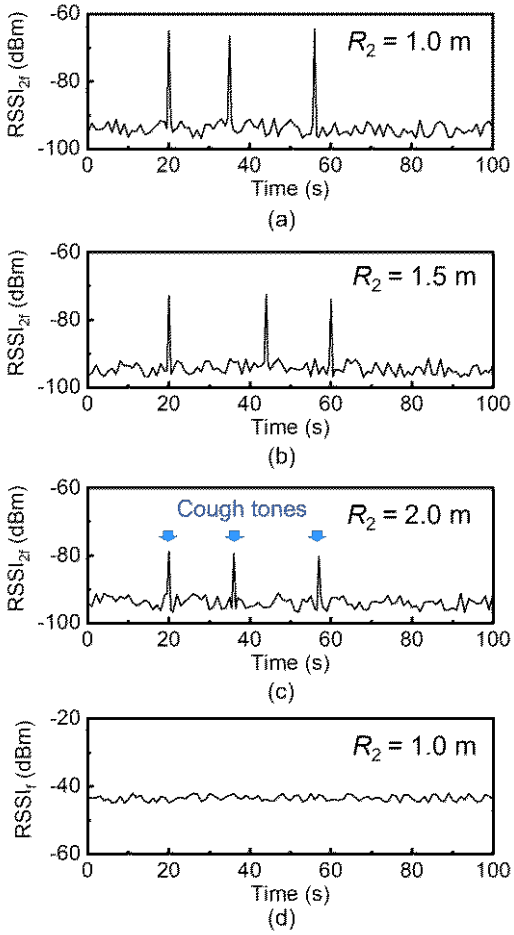

Fig. 9. Measured time series of harmonic RSSI at an interrogating distance of (a) 1.0 m, (b) 1.5 m, and (c) 2.0 m. (d) Similar to (a), but for a traditional passive backscattering tag.

frequency and pattern of cough can be obtained from the recorded time series of the second-harmonic RSSI (at 3.0 GHz). According to the Friis transmission equation, the second-harmonic RSSI (i.e., received power P_r) can be estimated as [51]:

$$\frac{P_r}{P_t}=\left(\frac{\lambda_0}{4\pi\sqrt{2R_1R_2}}\right)^4\times \frac{G_T(f_0)G_r(f_0,g)G_t(2f_0,g)G_R(2f_0)}{L_{sys}}\left|\hat{\boldsymbol{\rho}}_T\cdot\hat{\boldsymbol{\rho}}_r\right|^2\left|\hat{\boldsymbol{\rho}}_t\cdot\hat{\boldsymbol{\rho}}_R\right|^2 \quad (1)$$

where G_r is the realized gain of the meander-line antenna at f_0, G_t is the realized gain of the inverted-F antenna at $2f_0$, G_T (G_R) denote the realized gain of the reader's transmitter (sniffer), the antenna's realized gain is determined by its radiation efficiency η_e, reflection coefficient Γ_i, and directivity D_i as $G_i=\eta_e(1-|\Gamma_i|^2)D_i$, R_1 (R_2) is the distance between reader (sniffer) and the face mask, L_{sys} is the overall system loss including the conversion loss of the frequency doubler and the insertion loss in filters and transmission line, $\hat{\boldsymbol{\rho}}_i$ is the polarization of the i-th antenna, and $\left|\hat{\boldsymbol{\rho}}_i\cdot\hat{\boldsymbol{\rho}}_j\right|^2$ is the polarization loss factor (PLF) per trip. When an antenna is very close to the human head, the dielectric loading effect will vary the antenna impedance Z_a and return loss given by $\Gamma_i=(Z_a-Z_{in})/(Z_a+Z_{in})$, where Z_{in} is the input impedance of the transponder. This will in turn modulate the realized gains G_r and G_t, such that the detected second-harmonic signal [Eq. (1)] is sensitively dependent on the air gap between the mask and the human head. In other words, when an antenna is embedded in the smart mask, its realized gain during coughing $G_i(g)$ can be related to that in the non-cough case $G_i(0)$ by a factor of $\left(1-\Gamma_i(g)\Gamma_i^*(g)\right)/\left(1-\Gamma_i(0)\Gamma_i^*(0)\right)$; here, we note that the antenna's radiation pattern and directivity D_i could also be slightly varied. Some important parameters in the measurement include: P_t = 20 dBm, R_1 = R_2 = 1 m, G_T = 12.5 dBi at 1.5 GHz, and G_R = 15.0 dBi at 3.0 GHz. From Eq. (1), it is evident that under a fixed transmitted power P_t, the received power P_r is proportional to the realized gain G_r and G_t of the antennas, which have been demonstrated to be sensitive to the occurrence of cough, as can be seen in Fig. 5. In short, when the user wearing the harmonic mask is at rest (which corresponds to the OFF state of the harmonic tag), resonant frequencies of antennas do not match to 1.5 GHz and 3.0 GHz, leading to a very small G_r and G_t, and thus low harmonic RSSI, as can be seen in Fig. 8(a). On the other hand, the occurrence of cough

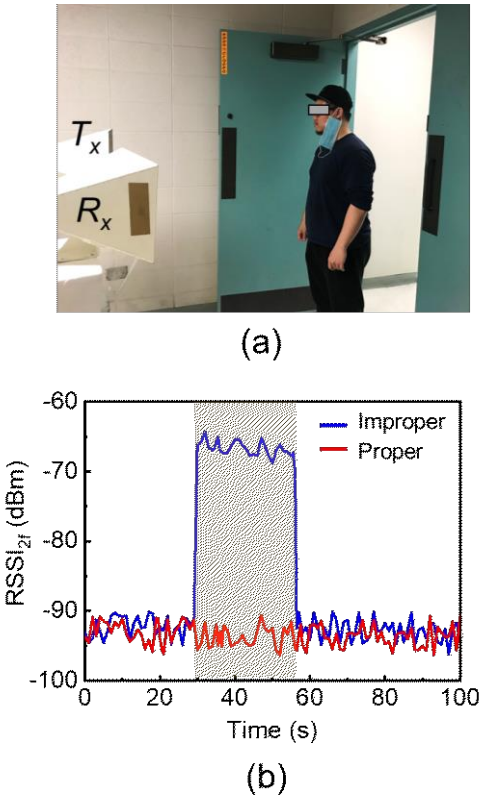

Fig. 10. (a) Experimental configuration for detecting the mask wearing condition. (b) Measured time series of harmonic RSSI, in which the continuous existence of the second harmonic signal indicates wrong mask-wearing.

can dynamically reconfigure the resonant frequencies of the meander-line antenna and the inverted-F antenna to 1.5 GHz and 3.0 GHz. Therefore, a harmonic RSSI peak can be detected, as can be seen in Fig. 8(b). Consequently, the cough events can be continuously monitored by analyzing the harmonic RSSI pattern over time. We note that in both cough and non-cough cases, due to the serious crosstalk and clutters, a backscattered signal was always detected at the fundamental frequency.

Next, we validate robustness and effectiveness of our platform by performing the real-time cough monitoring in the noisy environment. The harmonic RSSI is recorded over 100 s. The results reported in Fig. 9(a) shows that the proposed smart face mask enables robust, accurate, and real-time cough monitoring. Figs. 9(b) and(c) present the measured time series of the second-harmonic RSSI at different interrogation distances [see measurement configuration in Fig. 7]; here, except for the tag-to-sniffer distance (R_2), all the other measurement conditions remain the same. It is evidently seen that the pattern of transient response of the smart face mask remains unchanged, regardless of the interrogation distance. Therefore, we conclude that the proposed wearable device may provide an accurate cough monitoring with excellent robustness and reliability. We should also note that with the same setup, robust detection can be achieved with an interrogation distance R_2 =3.0 m and a noise floor of -90 dBm. The maximum range can be further increased by using high-resolution spectrum analyzer (which can be down to -120 dBm) or by performing

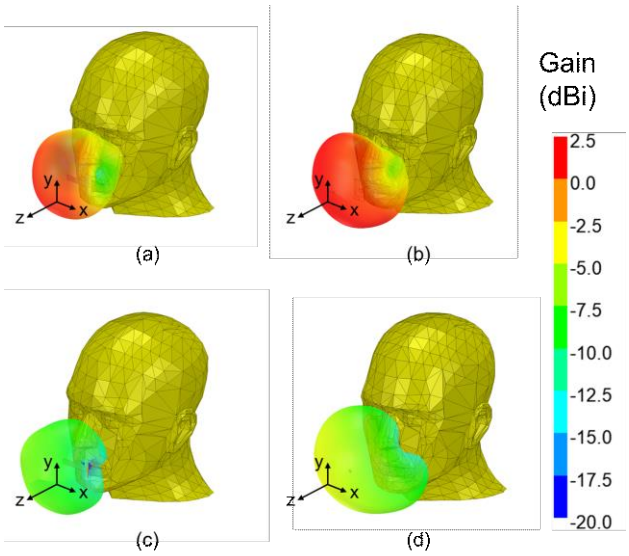

Fig. 11. Radiation pattern of (a) the meander-line antenna at 1.5 GHz and (b) the IFA at 3.0 GHz situated nearby the human head, with an air gap of 10 mm. (c), (d): are similar to (a) and (b), but with antennas conformal to the human face, i.e., with an air gap of ~0 mm.

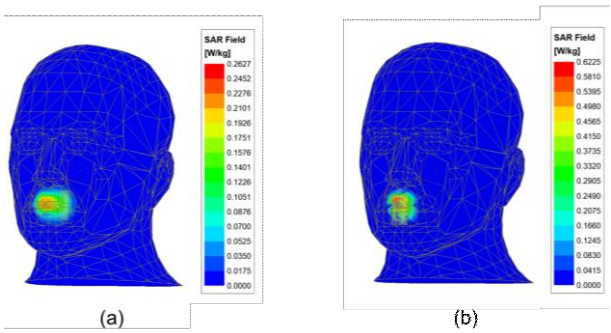

Fig. 12. SAR distributions of (a) the meander-line antenna and (b) IFA placed conformally on the human head.

data correction using the time-domain gating or intelligent algorithms. For a comparison, we also employed the traditional passive antenna sensor to wirelessly monitor the same cough event. This antenna sensor consists of a microstrip meander-line antenna terminated by a 50 Ω match load. The measured variations of RSSI at 1.5 GHz is presented in Fig. 9(d). Obviously, although the RSSI is still modulated over time, the measured backscattered signal cannot be differentiated from the background noises sourced mainly from crosstalks and clutters. Therefore, it is clearly evident that the proposed harmonics-based wearable device may be a promising candidate for accurate real-time monitoring of coughs.

Besides, our proposed smart face mask can operate as an indicator for mask wearing condition. In the same vein, the properly worn mask is subject to remarkable frequency shift due to parasitics (i.e., a dielectric loading effect) sourced from the human body, resulting in an undetectable second harmonic signal. On the other hand, if one wears the mask incorrectly [Fig. 10(a)], the air gap between the harmonic mask and face will lead to a successive second harmonic series in the time domain. Fig. 10(b) reports the time-series RSSI received from

the smart mask that is worn incorrectly, showing a continuous appearance of second-harmonic signals as an alert to improper use of face mask.

At last, the performance of the proposed antenna on a 3-D human head model is analyzed. The bioelectromagnetic model used in the simulation is a male head from the HFSS library. The antennas are placed in the proximity of the human mouth with an air gap g = 10 and 0 mm, which respectively mimic the on and off states in Fig. 8. Fig. 11 reports the 3D radiation pattern of the meander-line antenna and IFA with the existence of the human head. From Fig. 11, it is seen that the radiated power is remarkably reduced when the antennas are placed conformally on the human face, due to the effect of dielectric loading (i.e., human tissues). According to our simulation results, the realized gain of the antennas with air gap g = 10 mm are 1.9 dBi and 2.3 dBi, which are comparable to the results in free space, as shown in Figs. 11 (a) and (b). However, when the mask is situated at the head, the realized gain of the meander-line antenna drops to -7.4 dBi [Fig. 11(c)] and that of the IFA drops to -5.1 dBi [Fig. 11(d)], due primarily to the frequency shift under the effect of dielectric loading. Note that the antennas themselves have quite low conduction and dielectric losses, thanks to the relatively small loss tangent of the Roger substrate, when compared to other flexible alternatives such as PDMS or textile [52]-[54].

In order to ensure the conformance to safety regulations, the specific absorption rate (SAR) values are also evaluated and averaged over 1 g of biological tissue based on the IEEE/IEC 62704-4 standard. Considering that our antennas are integrated and utilized as a fully-passive device, electromagnetic radiations are sourced from scattering and reception by the meander-line antenna (1.5 GHz), and the emission at the IFA (3 GHz) ; the input power in our SAR simulation was set to 5 dBm. Fig. 12 plots the SAR distributions for each antenna at their resonance frequencies with the gap ~ 0 mm. It can be seen from Fig. 12 that the maximum averaged SAR obtained is only 0.26 W/kg for the meander-line antenna at 1.5 GHz [Fig. 12(a)] and 0.62 W/kg for the IFA at 3.0 GHz [Fig. 12(b)]; such values are much lower than the European standard threshold of 2 W/kg.

Finally, it is worthwhile mentioning that in practical applications, talking and laughing may introduce an air gap of g ~ 10 mm, which could potentially lead to false detection of cough events. However, the classification between coughing, talking and laughing could be achieved by means of data post-processing of the measured data, e.g., applying the pattern recognition algorithm onto the time series of harmonic RSSI signal. Besides, such a problem can be overcome by performing the hybrid simulation of antenna radiation characteristics associated with Maxwell's equations and variations in the shape of the face mask associated with the fluid dynamics governed by the Navier-Stokes equations. The size of this passive smart face mask can be further squeezed by utilizing compact and directive antennas, such as Huygens dipoles, and the portable RF signal generator and spectrum analyzer. In addition, this passive smart face mask can also be designed and manufactured based on the flexible, stretchable and porous (breathable) materials, such as patterned AgNWs networks on the elastomer substrate. This will provide more comfortable and user-friendly wireless cough monitoring, which could find various applications in monitoring a wide range of health conditions and behaviors.

IV. Conclusion

In this paper, we have demonstrated a lightweight, low-profile and fully-passive harmonic tag embedded in a face mask for the continuous, real-time wireless cough monitoring. Specifically, in the scheme of harmonics-based sensing, the proposed wearable sensor is capable of measuring the frequency and pattern of cough in the far zone of the cluttered indoor environment. Moreover, comparing to traditional cough monitoring approaches based on passive antenna sensors or backscatter RFIDs, the proposed smart face mask could offer much improved accuracy, robustness, and reliability in real-life applications, potentially benefiting the rapid healthcare tests (e.g., point-of-care testing and driver through tests), telemedicine, healthcare internet-of-things, and biomedical and clinical research.

V. References

[1] K. F. Chung, "Methods of assessing cough and antitussives in man," *Pulmonary Pharmacol.,* vol. 9, pp. 373-377, 1996.

[2] R. S. Irwin, F. J. Curley, and C. L. French, "Chronic cough. The spectrum and frequency of causes, key components of the diagnostic evaluation, and outcome of specific therapy," *A. Rev. Respiratory Disease,* vol. 141, no. 3, pp. 640-647, 1990.

[3] C. L. French, R. S. Irwin, F. J. Curley, and C. J. Krikorian, "Impact of chronic cough on quality of life," *Arch. Intern. Med.,* vol. 158, no. 15, pp. 1657-1661, 1998.

[4] R. S. Irwin, C. T. French, and K. E. Fletcher, "Quality of life in coughers," *Pulmonary Pharmacol.*, vol. 15, no. 3, pp. 283-286, 2002.

[5] H. Hong, L. Zhang, H. Zhao, H. Chu, C. Gu, M. Brown, et al., "Microwave sensing and sleep: Noncontact sleepmonitoring technology with microwave biomedical radar," *IEEE Microw. Mag.*, vol. 20, no. 8, pp. 18-29, Aug. 2019.

[6] Y. Y. Zheng, Y. T. Ma, J. Y. Zhang and X. Xie, "COVID-19 and the cardiovascular system," *Nat. Rev. Cardiol.,* 2020.

[7] H. A. Bickerman and S. E. Itkin, "The effect of a new bronchodilator aerosol on the air flow dynamics of the maximal voluntary cough of patients with bronchial asthma and pulmonary emphysema," *Journal of Chronic Diseases*, vol. 8, no. 5, pp. 629-638, 1958.

[8] C. Li, V. M. Lubecke, O. Boric-Lubecke, and J. Lin, "A review on recent advances in Doppler radar sensors for noncontact healthcare monitoring," *IEEE Trans. Microw. Theory Techn.*, vol. 61, no. 5, pp. 2046-2060, May. 2013.

[9] C. Li, Z. Peng, T. Y. Huang, T. Fan, F. K. Wang, T. S. Horng, et al., "A review on recent progress of portable short-range noncontact microwave radar systems," *IEEE Trans. Microw. Theory Techn.*, vol. 65, no. 5, pp. 1692-1706, May. 2017.

[10] G. Wang, C. Gu, T. Inoue, and C. Li, "A hybrid FMCW-interferometry radar for indoor precise positioning and versatile life activity monitoring," *IEEE Trans. Microw. Theory Techn.*, vol. 62, no. 11, pp. 2812-2822, Nov. 2014.

[11] W. T. Goldsmith, A. M. Mahmoud, J. S. Reynolds, W. G. Mckinney, et al., "A system for recording high fidelity cough sound and airflow characteristics," *Ann. Biomed. Eng.,* vol. 38, no. 2, pp. 469-477, 2010.

[12] S. Ren, Y. Shi, M. Cai, and W. Xu, "Influence of secretion on airflow dynamics of mechanical ventilated respiratory system," *IEEE/ACM Trans. Comput. Biol. Bioinform.,* vol. 15, no. 5, pp. 1660-1668, 2018.

[13] S. Ren, M. Cai, Y. Shi, W. Xu, and X. D. Zhang, “Influence of bronchial diameter change on the airflow dynamics based on a pressure-controlled ventilation system,” *Int. J. Numer. Method Biomed. Eng.,* vol. 34, no. 3, 2018.

[14] Y. Hu, E. G. Kim, G. Cao, S. Liu, and Y. Xu, “Physiological acoustic sensing based on accelerometers: a survey for mobile healthcare,” *Ann. Biomed. Eng.,* vol. 42, no. 11, p. 2264-2277, 2014.

[15] S. Subburaj, L. Parvez, and T. G. Rajagopalan, “Methods of recording and analysing cough sounds,” *Pulmonary Pharmacol.,* vol. 9, pp. 269-279, 1996.

[16] P. Munyard, C. Busst, R. Logan-Sinclair, and A. Bush, “A new device for ambulatory cough recording,” *Pediatr. Pulmonol.,* vol. 18, no. 3, pp. 178-186, 1994.

[17] L. B. Sun, Y. Li, Z. J. Zhang, and M. F. Iskander, “Low-Cost Compact Circularly Polarized Dual-Layer PIFA for Active RFID Reader,” *IEEE Trans. Antennas Propag.*, vol. 67, no. 1, pp. 681-686, Jan 2019.

[18] L. Chang, H. Wang, Z. J. Zhang, Y. Li, and Z. H. Feng, “Compact Single-Feed Dual-Mode Antenna for Active RFID Tag Application,” *IEEE Trans. Antennas Propag.*, vol. 63, no. 11, pp. 5190-5194, Nov 2015.

[19] C. Liu, J. Xiong, L. Cai, L. Feng, and X. Chen, et al., “Beyond respiration: Contactless sleep sound-activity recognition using RF signals,” *in Proceedings of the ACM on Interactive, Mobile, Wearable and Ubiquitous Technologies (ACM UbiComp).,* vol. 3, no. 3, pp. 1-22, 2019.

[20] P. Sharma, X. Hui and E. C. Kan, “A wearable RF sensor for monitoring respiratory patterns,” *in 41st Annual International Conference of the IEEE Engineering in Medicine and Biology Society (EMBC),* pp. 1217-1223, 2019.

[21] X. Hui and E. C. Kan, “Collaborative reader code division multiple access in the harmonic RFID system”, *IEEE J. Radio Freq. Identification*, Art. 2469-7281, July 2018.

[22] L. Zhu, and P. Y. Chen, “A compact, zero-power and low-noise harmonic-transponder for liquid and moisture sensing,” in 2019 *IEEE International Symposium on Antennas and Propagation and USNC-URSI Radio Science Meeting*, Atlanta, GA, USA, USA, 2019.

[23] L. Zhu, N. Alsaab, M. M. C. Cheng and P. Y. Chen, “A zero-power ubiquitous wireless liquid-level sensor based on microfluidic-integrated microstrip antenna,” *IEEE J. Radio Freq. Identification,* vol. 4, no. 3, pp. 265-274, 2020.

[24] L. Zhu, M. Farhat, Y. C. Chen, K. N. Salama and P. Y. Chen, “A compact, passive frequency-hopping harmonic sensor based on a microfluidic reconfigurable dual-band antenna,” *IEEE Sens. J.,* vol. 20, no. 21, pp. 12495-12503, 2020.

[25] X. Gu, S. N. N, L. Guo, S. Hemour, and K. Wu, “Diplexer-based fully passive harmonic transponder for sub-6-GHz 5G-compatible IoT applications,” *IEEE Trans. Microw. Theory Techn.,* vol. 67, no. 5, pp. 1675-1687, 2019.

[26] F. Yu, K. G. Lyon, and E. C. Kan, "A novel passive rfid transponder using harmonic generation of nonlinear transmission lines," *IEEE Trans. Microw. Theory Techn.,* vol. 58, no. 12, pp. 4121-4127, Dec 2010.

[27] Y. F. Ma and E. C. Kan, "Accurate indoor ranging by broadband harmonic generation in passive nltl backscatter tags," *IEEE Trans. Microw. Theory Techn.,* vol. 62, no. 5, pp. 1249-1261, May 2014.

[28] D. Mascanzoni and H. Wallin, “The harmonic radar: A new method of tracing insects in the fields,” *Ecol. Entomol.*, vol. 11, pp. 387-390, 1986.

[29] K. Rasilainen, J. Ilvonen, A. Lehtovuori, J. M. Hannula, and V. Viikari, “Harmonic Transponders: Performance and Challenges,” *Progress in Electromagnetics Research M*, vol. 41, pp. 139-147, 2015.

[30] K. Rasilainen, J. Ilvonen, A. Lehtovuori, J. M. Hannula, and V. Viikari, “On Design and Evaluation of Harmonic Transponders,” *IEEE Trans. Antennas Propag.*, vol. 63, no. 1, pp. 15-23, Jan 2015.

[31] V. Palazzi, F. Alimenti, C. Kalialakis, P. Mezzanotte, A. Georgiadis, and L. Roselli, “Highly Integrable Paper-Based Harmonic Transponder for Low-Power and Long-Range IoT Applications,” *IEEE Antennas Wireless Propag. Lett.*, vol. 16, pp. 3196-3199, 2017.

[32] X. A. Hui, Y. F. Ma, and E. C. Kan, "Code division multiple access in centimeter accuracy harmonic rfid locating system," *IEEE J. Radio Freq. Identification,* vol. 1, no. 1, pp. 51-58, Mar 2017.

[33] X. N. Hui and E. C. Kan, "Radio ranging with ultrahigh resolution using a harmonic radio-frequency identification system," *Nat. Electron.,* vol. 2, no. 3, pp. 125-131, Mar 2019.

[34] B. G. Colpitts and G. Boiteau, “Harmonic radar transceiver design: miniature tags for insect tracking,” *IEEE Trans. Antennas Propag.,* vol. 52, no. 11, pp. 2825-2832, 2004.

[35] L. Zhu, N. Alkhaldi, H. M. Kadry, S. L. Liao, and P. Y. Chen, “A compact hybrid-fed microstrip antenna for harmonics-based radar and sensor system,” *IEEE Antennas Wireless Propag. Lett.,* vol. 17, no. 12, pp. 2444-2448, 2018.

[36] J. R. Riley, A. D. Smith, D. R. Reynolds, and A. S. Edwards, “Tracking bees with harmonic radar,” *Nature,* vol. 379, pp. 29-30, 1996.

[37] V. Palazzi, F. Alimenti, P. Mezzanotte, G. Orecchini, and L. Roselli, “Zero-power, long-range, ultra low-cost harmonic wireless sensors for massively distributed monitoring of cracked walls,” *in IEEE MTT-S Int. Microw. Symp. Dig.*, Honolulu, HI, USA, Jun, 2017.

[38] C. Cho, X. H. Yi, D. Li, Y. Wang, and M. M. Tentzeris, “Passive wireless Frequency doubling antenna sensor for strain and crack sensing,” *IEEE Sens. J.,* vol. 16, no. 14, pp. 5725-5733, 2016.

[39] D. Ahbe, S. Beer, T. Zwick, Y. Wang, and M. M. Tentzeris, “Dual-band antennas for frequency-doubler-based wireless strain sensing,” IEEE Antennas Wireless Propag. Lett., vol. 11, pp. 216-219, 2012.

[40] V. Palazzi et al., “Demonstration of a chipless harmonic tag working as crack sensor for electronic sealing applications,” *Wireless Power Transfer*, vol. 2, no. 2, pp. 78-85, Sep 2015.

[41] V. Palazzi, F. Alimenti, P. Mezzanotte, G. Orecchini and L. Roselli, “Zero-power, long-range, ultra low-cost harmonic wireless sensors for massively distributed monitoring of cracked walls,” 2017 *IEEE MTT-S International Microwave Symposium (IMS)*, 2017, pp. 1335-1338,

[42] A. Lazaro, R. Villarino, and D. Girbau, “A passive harmonic tag for humidity sensing,” *Int. J. Antennas Propag.,* p. 670345, 2014.

[43] H. Huang, P. Y. Chen, C. H. Hung, R. Gharpurey, and D. Akinwande, “A zero power harmonic transponder sensor for ubiquitous wireless μL liquid-volume monitoring,” *Sci. Rep.,* vol. 6, p. 18795, 2016.

[44] M. Hajizadegan, M. Sakhdari, L. Zhu, Q. S. Cui, H. Y. Huang, M. C. Cheng, et al, “Graphene sensing modulator: Toward low-noise, self-powered wireless microsensors,” *IEEE Sens. J.,* vol. 17, no. 22, pp. 7239-7247, 2017.

[45] X. Hui and E. C. Kan, “Monitoring vital signs over multiplexed radio by near-field coherent sensing,” *Nat. Electron.,* vol. 1, no. 1, pp. 74-78, 2018.

[46] L. Zhu, H. Huang, M. M. C. Cheng and P. Y. Chen, “Compact, flexible harmonic transponder sensor with multiplexed sensing capabilities for rapid, contactless microfluidic diagnosis,” *IEEE Trans. Microw. Theory Tech.,* vol. 68, no. 11, pp. 4846-4854, 2020.

[47] A. Abdelnour, A. Lazaro, R. Villarino, D. Kaddour, S. Tedjini and D. Girbau, “Passive harmonic RFID system for buried assets localization,” *sensors,* vol. 18, no. 11, p. 3635, 2018.

[48] C. Gao, T. Wei, F. Duewer, Y. Lu, and X. D. Xiang, “High spatial resolution quantitative microwave impedance microscopy by a scanning tip microwave near-field microscope,” *Appl. Phys. Lett.,* vol. 71, pp. 1872-1874, 1997.

[49] H. Huang, P. S. Zhao, P. Y. Chen, Y. Ren, X. Liu, et al., “RFID tag helix antenna sensors for wireless drug dosage monitoring,” *IEEE J. Transl. Eng. Health Med.,* vol. 2, pp. 1-8, 2014.

[50] *Keysight PathWave Advanced Design System (ADS), Keysight Technol.*, Santa Rosa, CA, USA, 2020.

[51] J. A. Shaw, “Radiometry and the Friis transmission equation,” Am. J. Phys., vol. 81, no. 1, pp. 33-37, 2013.

[52] Zhi Hao Jiang, Donovan E. Brocker, Peter E. Sieber, and Douglas H. Werner, “A Compact, Low-Profile Metasurface-Enabled Antenna for Wearable Medical Body-Area Network Devices,” *IEEE Trans. Antennas Propag.*, Vol. 62, No. 8, pp. 4021 - 4030, Aug. 2014.

[53] Zhi Hao Jiang, Zheng Cui, Taiwei Yue, Yong Zhu, and Douglas H. Werner, “Compact, Highly Efficient, and Fully Flexible Circularly Polarized Antenna Enabled by Silver Nanowires for Wireless Body-Area Networks,” *IEEE Transactions on Biomedical Circuits and Systems,* Vol. 11, No. 4, pp. 920 - 932, May 2017

[54] Z. X. Hu, C. X. Chen, Z. H. Zhou, and Y. Li, "An Epsilon-Near-Zero-Inspired PDMS Substrate Antenna With Deformation-Insensitive Operating Frequency," *IEEE Antennas Wireless Propag. Lett.*, vol. 19, no. 9, pp. 1591-1595, Sept 2020.